

Article

Characterization of 2D Electrical Feedback Flow Control Valve

Quanchao Dai , Jiantao Zhao, Sheng Li * and Wenang Jia

College of Mechanical Engineering, Zhejiang University of Technology, Hangzhou 310023, China

* Correspondence: lishengjx@zjut.edu.cn; Tel.: +86-139-5710-1556

Abstract: We proposed a novel 2D electric feedback flow control valve to solve the problem of low integration and control accuracy of flow control valves. The torque motor of the valve drives the 2D piston to rotate, and the rotational motion is converted to axial motion and drives the spool. The differential pressure feedback rod on the valve body can accurately measure the differential pressure of the oil inlet and outlet and cooperate with the spool displacement to form a closed loop of flow. This loop of flow then overcomes the influence of the valve port's load change on the flow. We first established the mathematical model of the valve, obtained the transfer function, and performed the stability analysis. Then, we used AMESim as a platform for simulation analysis. Finally, we conducted the experimental verification of the valve. The verification showed the following characteristics of the valve. The hysteresis loop is 4.4%. The linearity is 1.6%. The response time is about 44 ms. The amplitude bandwidth is about 17 Hz. The phase bandwidth is about 28 Hz. The valve's steady-state flow error is less than 8%, suggesting its broad application prospect in the aerospace and military fields.

Keywords: 2D valve; flow valve; stable flow; dynamic and static characteristics; AMESim simulation; experimental study

1. Introduction



Citation: Dai, Q.; Zhao, J.; Li, S.; Jia, W. Characterization of 2D Electrical Feedback Flow Control Valve. *Machines* **2023**, *11*, 220. <https://doi.org/10.3390/machines11020220>

Academic Editor: Kim Tiow Ooi

Received: 5 January 2023

Revised: 31 January 2023

Accepted: 1 February 2023

Published: 2 February 2023



Copyright: © 2023 by the authors. Licensee MDPI, Basel, Switzerland. This article is an open access article distributed under the terms and conditions of the Creative Commons Attribution (CC BY) license (<https://creativecommons.org/licenses/by/4.0/>).

Electro-hydraulic servo valves with high control accuracy and fast response are generally used in fields that require high output power and high dynamic response, including aerospace, metallurgy, material testing, and military [1,2]. Micro valves, such as the vertically allocated SU-8 check valve formed by Mao et al. [3], can be used in less leaky microfluidic systems. The vertically allocated SU-8 check valve formed by photolithography has a limited overlap between an SU-8 cantilever and its valve seat, which was experimentally compared, and it was found that the fully overlapped SU-8 check valve possessed less leakage compared to the partially overlapped SU-8 check valve. Its diodicity (DI) is improved by about 2 times, from 1.7 to 3.5. If a stable flow rate is required, a pressure compensator must be used in conjunction with a flow sensor, which can form a closed-loop control of the flow rate [4–6]. However, pressure-compensated flow control valves are often disadvantaged due to low control accuracy, large flow overshoot, and large energy losses [7].

Researchers have worked extensively to improve the performance of electrohydraulic valves. Okhotnikov et al. [8] studied the steady-state flow state and hydraulic characteristics of rotating flow control valves for high-flow fluid systems. They used CFD simulations to predict the torque and pressure drop caused by steady-state flow and improved the controllable performance of the flow valves. Wang et al. [9] designed a mathematical model of a constant flow control valve to quantitatively analyze how the overflow area and gradient, among other factors, at the valve orifice, influence the valve characteristics. They further analyzed the mechanisms of these influences based on AMESim simulation. They found that adjusting the differential pressure compensator overflow area and gradient can significantly improve the static dynamics of the flow valve. Jin et al. [10] analyzed the force output of two proportional solenoids to minimize the variation of the current

force gain. They proposed a different control method (DCM) to reduce the effect of the nonlinearity of proportional solenoids on the performance of a proportional reversing valve. Their experimental results showed that compared to the normal control method, the DCM can greatly improve the frequency response of proportional reversing valves at small current input.

Milecki et al. [11] proposed a novel proportional valve, which outputs the flow proportionally to the sum of the steps of two stepper motors. Through modeling and simulation of the valve, they found that the stepper motors have significant overshoot and further proposed a special control algorithm to achieve a high positioning accuracy. Wang et al. [12] performed a theoretical analysis to compare a flow control valve with controlled pressure that they proposed with a traditional flow control valve. The experimental results showed that the valve has a wider range of differential pressure compensation; the output flow can vary from 44% to 100% of the rated flow and attempts to compensate for the effects of hydrodynamic forces. Li et al. [13] and others designed a liquid-controlled proportional flow control valve by optimizing the spool throttle slot. They stabilized the output flow by adding a pressure compensator to the proportional reversing valve that has a pressure compensation range of 0.3~0.7 MPa. Both studies [12,13] used pressure compensators to compensate for the differential pressure between the import and export to stabilize the flow. However, the pressure compensation ranges are narrow, and the control accuracy is poor.

Subsequently, Huang et al. [14] proposed a flow control valve with a pilot digital pressure compensator. The compensator detects the pressure drop at the pilot valve metering port with a pressure sensor and compensates for the pressure compensation. A comparative analysis of the theory and experiment supported the feasibility of the scheme. Based on the principle of pilot flow amplification of the Valvistor valve, Zhao et al. [15] eliminated the differential pressure compensator and the flow sensor in the main valve circuit and used proportional amplification of the main valve's pilot flow to control the main valve flow and reduce the pressure loss. Hao et al. [16] adjusted the pilot flow by changing the hydraulic pump speed to offset the flow fluctuations caused by the differential pressure changes.

However, many factors, such as pressure fluctuations, processing errors, and hydrodynamic forces [17–19], affect the amplification factor between the main flow and the inflow and directly affect the main valve flow, as the controlled object has a higher control accuracy. The 2D valve proposed by Ruan et al. [20,21] integrates the pilot and power stages of a traditional multi-stage valve into a spool with two degrees of freedom. This valve has only a simple structure but also excellent anti-pollution capability. The 2D electric feedback flow control valve designed on this basis achieves flow control by metering the differential pressure between the inlet and outlet and the spool displacement to ensure response speed. In this study, we describe the structure and operation principle of a 2D electric feedback flow control valve, establish the transfer functions of the pilot and power stages, simulate the valve as a whole using AMESim, and verify the valve through experiments.

2. Structure Principles

The 2D electric feedback flow control valve includes a torque motor, a main valve body, a differential pressure feedback rod, a damping piston, and some displacement sensor modules (Figure 1). The torque motor converts its angular displacement into axial displacement through the 2D piston that changes the valve opening. The differential pressure feedback rod can then be displaced in response to the change in pressure drop between the working port and the high-pressure port. The displacement sensors 1 and 2 integrated into the torque motor can feed back the displacement of the differential pressure feedback lever and the spool to the controller. The current flow rate at the working port is then calculated and compared with the input expected flow rate for the purpose of flow control.

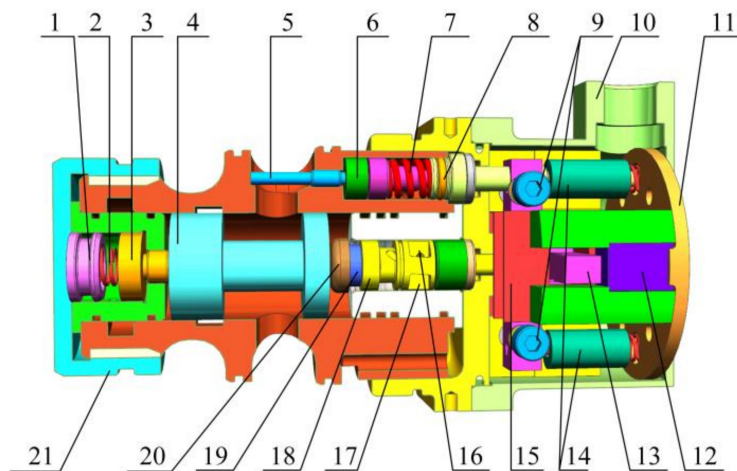


Figure 1. Schematic diagram of 2D electric feedback flow control valve. 1. plug; 2. reset spring; 3. damping piston; 4. main spool; 5. pressure-sensing piston; 6. differential-pressure-damping piston; 7. pressure-sensing spring; 8. seal; 9. zero adjustment screw; 10. torque motor housing; 11. torque motor bracket; 12. permanent magnet; 13. armature; 14. LVDT linear displacement sensor; 15. coil; 16. low-pressure groove; 17. high-pressure groove; 18. 2D piston; 19. thrust bearing; 20. bushing; 21. left end cap.

2.1. Working Principle of the 2D Piston

A schematic of the 2D piston structure is shown in Figure 2. The 2D piston is the key module of the 2D electrical feedback flow control valve. The piston consists of a high-pressure chamber, a sensitive chamber, an oblique groove, a high-pressure groove, and a low-pressure groove. When the torque motor is fed with the current to the output torque and drives the 2D piston to rotate, the overlapping area of the oblique groove and the high- and low-pressure grooves on the valve body changes. The changes in flow rate from the high-pressure chamber to the sensitive chamber result in changes in the pressure in the sensitive chamber. The spool loses balance, and the pressure difference between the sensitive and high-pressure chambers drives the spool to axial displacement.

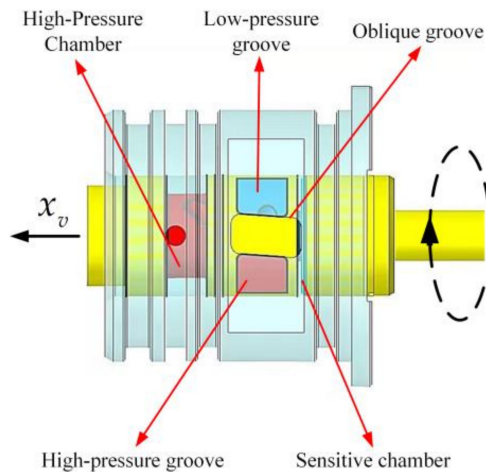


Figure 2. Schematic diagram of 2D piston rotation.

2.2. Differential Pressure Measurement Principle

In general, the differential pressure between the inlet and outlet of the flow valve is measured by a pressure sensor. However, on the one hand, as the servo valve works, the oil temperature rises, and the accuracy of the common pressure sensor will be significantly reduced. On the other hand, the pressure sensor would occupy extra space and increase the overall mass of the valve, making it unsuitable for small and low-mass working places.

Therefore, we designed the differential pressure feedback rod outside the valve body to reduce the number of components and the volume of the valve. The structure principle of the differential pressure feedback rod is shown in Figure 3.

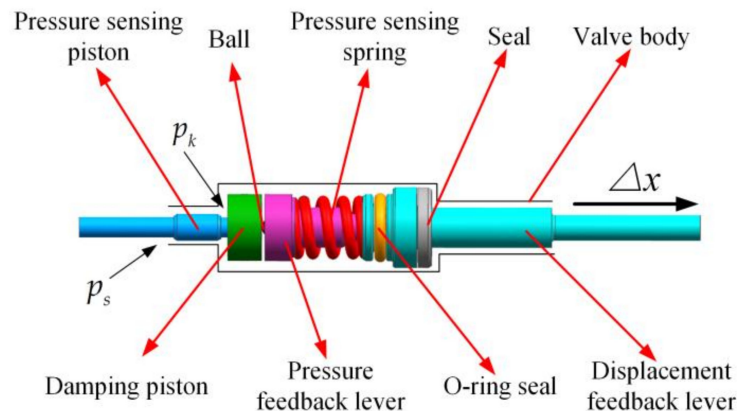


Figure 3. Schematic diagram of differential pressure feedback rod.

The pressure-sensing piston is connected to the pressure feedback rod through the ball. The right side of the displacement feedback rod is connected to the LVDT linear displacement sensor, which can feed the displacement collection to the controller. The controller can calculate the current import and export pressure difference according to the relationship between the import and export pressure differences and the displacement.

The force balance equation for the differential pressure feedback rod is

$$p_s A_i - p_k A_o = K_q \Delta x \quad (1)$$

where A_o is the effective force area on the right side of the pressure-sensing piston; A_i is the effective force area on the left side of the pressure-sensing piston; p_k is the oil outlet pressure; p_s is the oil inlet pressure; K_q is the pressure measuring spring stiffness; and Δx is the magnitude of the differential pressure feedback rod displacement.

The relationship between the differential inlet and outlet pressure Δp and the differential pressure feedback rod displacement Δx can be obtained as follows:

$$\Delta p = \frac{K_q \Delta x - p_s (A_i - A_o)}{A_o} \quad (2)$$

Initially, the differential pressure feedback rod is at the zero position. When the pressure at the work port decreases, the differential pressure feedback rod loses balance and starts to move to the right, driven by the pressure at the oil inlet. As the compression of the pressure-sensitive spring increases, the spring force gradually increases, and the differential pressure feedback rod reaches the balance again. When the pressure at the work port increases, the force on the right increases, and the differential pressure feedback rod is displaced to the left. This elongates the pressure-sensitive spring. In turn, the spring force gradually increases to bring the feedback rod back to balance again. The linear displacement sensor directly connected to the displacement feedback rod sends feedback on the collected displacement to the controller and calculates the differential pressure.

2.3. Working Principle of the Torque Motor

The structure principle of the torque motor is shown in Figure 4. The torque motor's components include an armature, a permanent magnet, and a coil. When no current is applied to the coil, the armature is at the zero position. When the torque motor is turned on, the coil produces the red magnetic flux due to the current (Figure 4). At air gaps 1 and 3, the blue flux produced by the permanent magnet is in the same direction as the red flux produced by the coil, while at air gaps 2 and 4, the fluxes are in different directions.

This difference causes the armature to lose balance and rotate to the output torque until it regains balance by the zeroing spring. If the current is passed in the opposite direction, the armature is subjected to a force exactly opposite to the above situation, and the torque and angle in the opposite direction will be output.

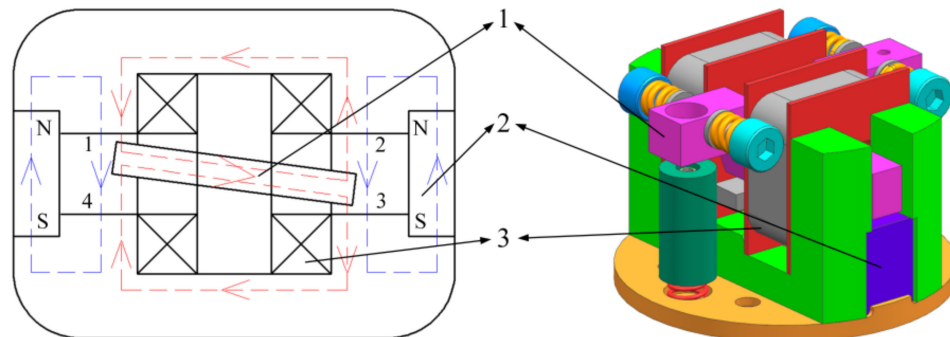


Figure 4. Torque motor schematic diagram. 1. armature; 2. permanent magnet; 3. coil.

2.4. Working Principle

Figure 5 illustrates the structure of the 2D electrical feedback flow control valve. The valve consists of a pilot stage 2D piston, a power stage spool, a differential pressure feedback rod, a damping piston, and a reset spring.

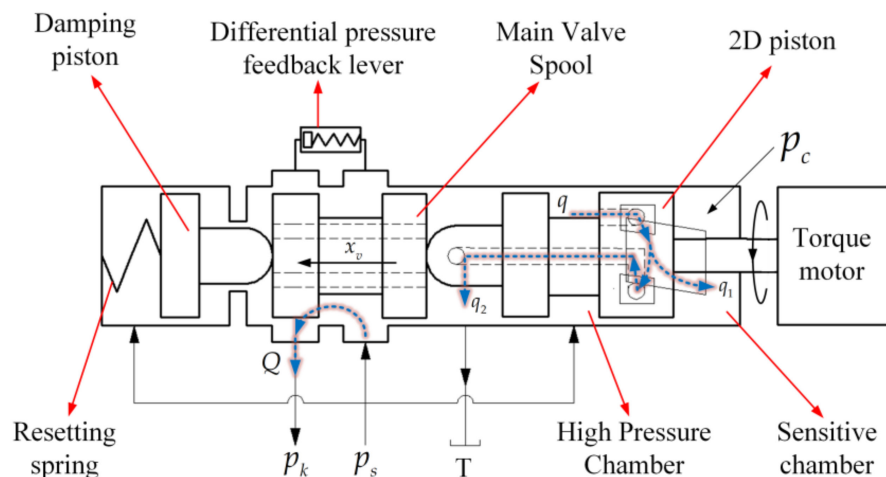


Figure 5. Structure principle of the 2D electric feedback flow regulating valve.

Initially, the valve opening is zero and the torque motor turning angle is zero, too. When the torque motor turns on the current and drives the 2D piston to turn counter-clockwise, the overlapping area between the high-pressure groove and the oblique groove increases. This drives the high-pressure oil that is flowing into the sensitive chamber on the right to increase, resulting in a higher pressure in the sensitive chamber. The spool moves axially to the left due to the pressure difference between the high-pressure and sensitive chambers. The reset spring is compressed. As the 2D piston moves axially, it also changes the size of the overlapping area between the high- and low-pressure grooves and the oblique groove. In turn, the overlapping area between the oblique and high-pressure grooves, the flow into the sensitive chamber, and the pressure in the sensitive chamber all decrease, and the pressure in the high-pressure chamber remains unchanged. Thus, the force on the spool reaches equilibrium again, and the spool reaches the designated position. The flow at the working port has increased. When the torque motor outputs in the opposite direction, the spool moves in the opposite direction; the overlapping area of the high-pressure groove and the oblique groove decreases, and the high-pressure oil flowing into the sensitive chamber decreases. This results in a lower pressure in the sensitive

chamber, and the spool is no longer balanced because of the force of axial movement to the right. As the 2D piston moves to the right, both the overlapping area of the high-pressure groove and the oblique groove and the pressure in the sensitive chamber gradually increase. The pressure in the sensitive chamber gradually increases, the pressure on the spool is rebalanced, and the flow rate of the working port is reduced. The 2D piston can amplify the smaller torque output from the torque motor into a greater hydraulic force and use it as a driving force to push the spool. It also has the characteristics of self-feedback.

When the load pressure of the working port changes, the differential pressure feedback rod starts to move axially because the force is imbalanced. The controller first collects the displacement of the differential pressure feedback rod through the displacement sensor. It then calculates the current pressure differences between the inlet and the outlet according to the relationship between the displacement of the differential pressure feedback rod and the differential pressure. It further calculates the current flow rate according to the pressure difference between the inlet and the outlet and the spool displacement collected by the displacement sensor. Then it compares the current flow rate with the expected input flow rate and adjusts the control signal through a control strategy to change the size of the torque motor angle. Finally, it adjusts the spool displacement of the 2D electric feedback flow control valve to ensure the stability of the output flow.

3. Stability Analysis

3.1. Transfer Function

To shorten the response time, we replaced the traditional high- and low-pressure hole structure with a high- and low-pressure groove structure. In the 2D piston rotation schematic (Figure 6), the torque motor shaft is connected to a 2D piston. When the torque motor rotates at an angle of θ , the overlap height of the high-pressure groove and the oblique groove on the 2D piston is:

$$h = R\theta \sin \beta + h_0 \quad (3)$$

where R is the radii of the 2D piston; β is the inclination angle of the oblique groove; θ is the rotation angle of the 2D piston rotation angle; and h_0 is the initial overlap height between the high-pressure trough and the inclined trough.

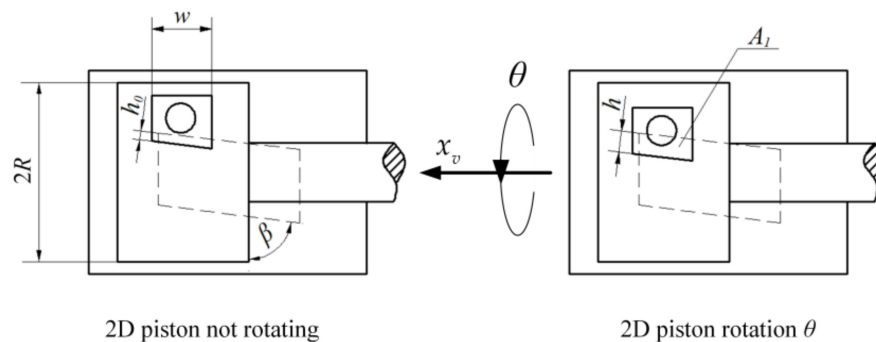


Figure 6. Schematic diagram of 2D piston rotation.

The 2D piston structure has a self-feedback link, that is, the axial displacement affects the overlap area of the high- and low-pressure grooves and the oblique grooves, which in turn affects the sensitive chamber pressure, causing the 2D piston to stop moving and reach a new equilibrium state. The relationship between the axial displacement of the spool and the change in the overlap height of the high- and low-pressure grooves of the 2D piston is:

$$\Delta h = R\theta \sin \beta - x_v \cos \beta \quad (4)$$

where x_v is the spool displacement.

The flow continuity equation in the sensitive chamber, without accounting for oil compression and leakage, is:

$$q_1 - q_2 = A_s \frac{dx_v}{dt} + \frac{V_c}{\beta_e} \frac{dp_c}{dt} \quad (5)$$

where q_1 is the flow rate from the high-pressure groove to the sensitive chamber via the oblique groove; q_2 is the flow rate of the sensitive chamber into the low-pressure groove through the inclined channel; A_s is the effective area of the sensitive chamber pressure on the 2D piston; V_c is the volume of the sensitive chamber; β_e is the bulk modulus of elasticity of the oil; and p_c is the pressure of the sensitive chamber.

$$q_1 = C_d A_1 \sqrt{\frac{2(p_s - p_c)}{\rho}} \quad (6)$$

where C_d is the flow coefficient; $A_1 = wh_0 / \sin \beta + R\theta w$ is the overlap area between the high-pressure groove and the oblique groove; w is the width of the high- and low-pressure grooves; and ρ is the fluid density.

$$q_2 = C_d A_2 \sqrt{\frac{2p_c}{\rho}} \quad (7)$$

where $A_2 = wh_0 / \sin \beta - R\theta w$ is the overlap area between the low-pressure groove and the oblique groove.

To improve the stability of the 2D electrical feedback flow control valve, we add a damped piston device, whose structure is shown in Figure 7.

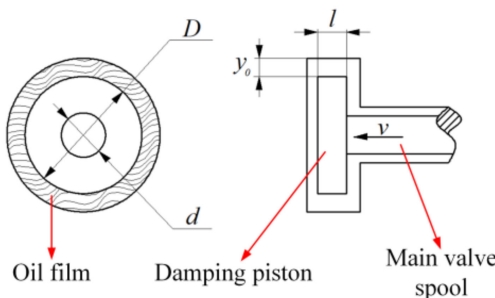


Figure 7. Schematic diagram of damping piston structure.

According to the literature [22], adding a damping piston does not change the force on the main spool, but only increases the velocity-dependent damping B_1 , whose size is:

$$B_1 = \frac{3\pi\mu l(D^2 - d^2 + 2y_0 D)(D^2 - d^2)}{4y_0^3 D} + \pi\mu l D \left(\frac{3(D^2 - d^2 + 2y_0 D)}{2y_0^2 D} + \frac{1}{y_0} \right) \quad (8)$$

where μ is the viscosity coefficient of the oil; l is the thickness of the damping piston; D is the large diameter of the damping piston; d is the small diameter of the damping piston; and y_0 is the thickness of the oil film.

The dynamic equilibrium equation of the spool can be expressed as:

$$p_c A_s - p_s A_r = m \frac{d^2 x_v}{dt^2} + (B_p + B_1) \frac{dx_v}{dt} + (K_v + K_f) x_v + F_L \quad (9)$$

where A_r is the effective area of the high-pressure chamber; m is the mass converted to the spool; B_p is the axial viscous damping coefficient; K_v is the axial spring stiffness; F_L is the external load force; K_f is the hydraulic equivalent stiffness.

According to Equations (3)–(9), and neglecting leakage and some non-linear factors, we obtain the control block diagram (Figure 8) and then obtain the transfer function.

$$\frac{x(s)}{\theta(s)} = \frac{R \tan \beta}{\frac{s^2 + \frac{2\zeta_n s}{\omega_n} + 1}{\cos \beta \cdot (K_1 / A_s)} + 1} \quad (10)$$

where ω_n is the intrinsic frequency of the 2D valve piston; K_1 is the flow gain coefficient of the 2D valve piston; and ζ_n is the damping ratio of the 2D valve piston.

$$\omega_n = \sqrt{\frac{\beta_e A_s^2}{m V_c}} \quad (11)$$

$$K_1 = 2C_d w \sqrt{\frac{p_s}{\rho}} \quad (12)$$

$$\zeta_n = \frac{\sqrt{\frac{A_s^2 \beta_e}{m V_c}}}{2A_s^2} \left(\frac{(B_p + B_1)V_c}{\beta_e} + mK_2 \right) \quad (13)$$

where K_2 is the coefficient of pressure flow gain of the 2D valve piston.

$$K_2 = \frac{2C_d h_0 w}{\sqrt{\rho p_s}} \quad (14)$$

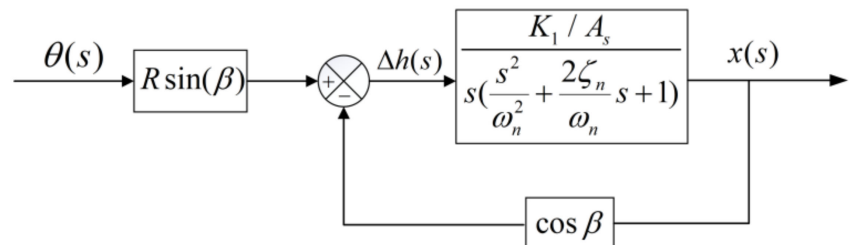


Figure 8. Control block diagram of 2D piston.

Based on the known 2D piston displacement (spool displacement), the relationship between the working port flow and spool displacement can be obtained according to the following slide valve orifice flow formula:

$$Q = C_d \omega x_v \sqrt{\frac{2\Delta p}{\rho}} \quad (15)$$

where Q is the valve port flow; ω is the gradient of the valve port through-flow area; and Δp is the differential inlet and outlet pressure.

3.2. Stability Analysis

According to the transfer function shown in Equation (10), the characteristic root equation can be obtained as:

$$\frac{s^3}{\omega_n^2} + \frac{2\zeta_n s^2}{\omega_n} + s + \cos \beta \cdot (K_1 / A_s) = 0 \quad (16)$$

By substituting the expressions of ω_n and ζ_n into Equation (13), the characteristic equation can be rewritten as:

$$\frac{mV_c}{\beta_e A_s^2} s^3 + \frac{\left(\frac{(B_p+B_1)V_c}{\beta_e} + mK_2\right)s^2}{A_s^2} + s + \cos \beta \cdot (K_1/A_s) = 0 \quad (17)$$

According to the Routh stability criterion, we obtain:

$$\frac{(B_p + B_1)V_c}{\beta_e} + mK_2 > \frac{mV_c K_1 \cos \beta}{\beta_e A_s} \quad (18)$$

After substituting the expressions of K_1 and K_2 into Equation (17) and performing term shifting, we obtain:

$$\frac{2C_d w h_0}{\sqrt{\rho p_s}} > \frac{2C_d m V_c w \cos \beta}{mA_s \beta_e} - \frac{(B_p + B_1)V_c A_s}{mA_s \beta_e} \quad (19)$$

From Equation (19), increasing the width of the high- and low-pressure grooves and the initial overlap height of the high- and low-pressure grooves can improve the stability of the 2D valve. However, this increase will lead to an increase in its leakage. Increasing the damping piston can increase the velocity-related damping without other negative effects, thus improving the overall stability of the 2D valve.

The values of the constant parameters used to calculate the equations are listed in Table 1. The set of interpretations of all parameters in this paper is shown in Appendix A.

Table 1. Constant parameters used for calculation formulas.

Parameters	Values
Oil density $\rho / (\text{kg} \cdot \text{m}^{-3})$	860
Absolute viscosity of oil $\mu / (\text{Pa} \cdot \text{s})$	0.03956
Maximum flow rate coefficient C_d	0.62
Inclined trough inclination angle $\beta / {}^\circ$	84
Bulk modulus of elasticity β_e / MPa	700
2D piston radii R / mm	6

4. AMESim-Based Modeling and Simulation

4.1. Simulation Model Building

Figure 9 displays a block diagram of the closed-loop control of the 2D electric feedback flow control valve flow, where the current inlet and outlet pressure difference is calculated by the relationship between the differential pressure feedback rod displacement and differential pressure shown in Equation (2). The spool displacement is collected by the displacement sensor connected to the spool. Based on the known spool displacement and the size of the differential pressure between the inlet and the outlet, the current flow rate can be calculated using Equation (15) to perform the feedback control.

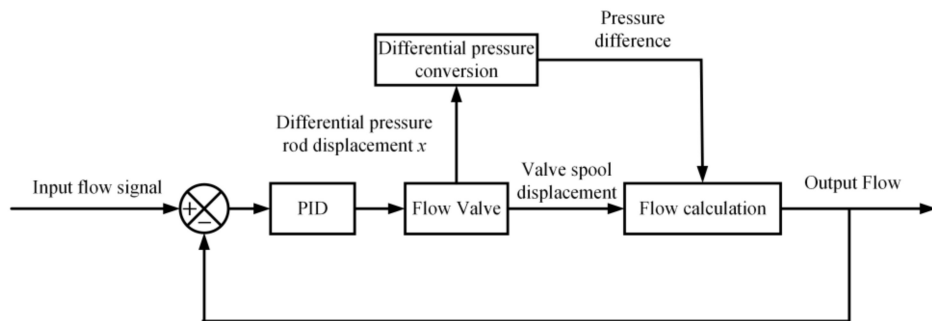


Figure 9. Flow feedback control block diagram.

The overall simulation model of the 2D electrical feedback flow control valve is shown in Figure 10. The torque motor as the electrical-mechanical converter is the first stage of the overall model. In the second stage, the 2D piston will convert the torque motor's angular signal into axial displacement. The main valve body is the third stage, which converts the axial displacement into flow output. The work port load can be simulated by adjusting different signal sources to simulate the load variations according to the needs.

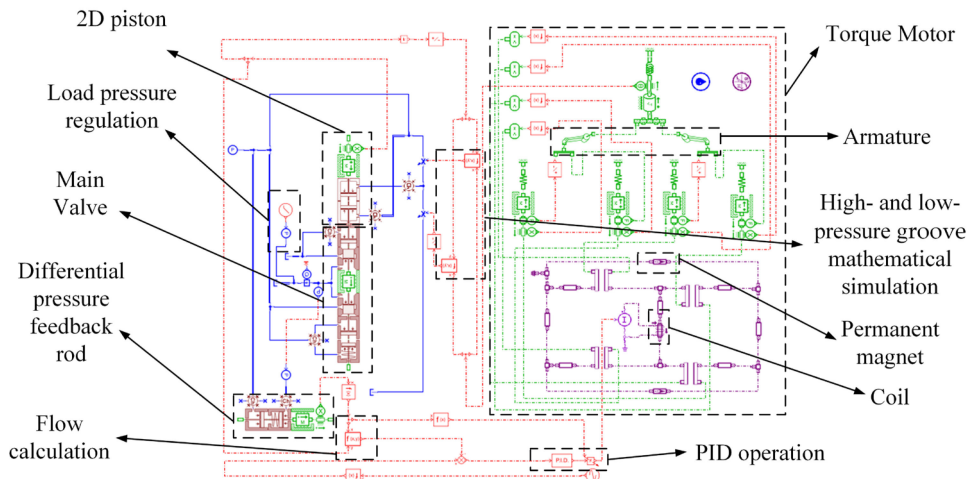


Figure 10. Simulation model of the 2D electric feedback flow control valve.

AMESim simulation key parameter settings are shown in Table 2.

Table 2. Key parameters of AMESim simulation.

Parameters	Values
Oil source temperature/°C	20
Oil density/(kg·m ⁻³)	860
System input oil pressure/MPa	9
Absolute viscosity of oil/(Pa·s)	0.03956
Valve spool diameter/mm	25
Valve spool quality/g	104
Maximum flow rate coefficient	0.62
Inclined trough inclination angle/°	84
Sensitive chamber area/mm ²	93.46
Initial overlap height/mm	0.005
Magnetic pole area/mm ²	32.5
Number of turns of coils	500
Bulk modulus of elasticity/MPa	700

4.2. Step Response Characteristic Analysis

Based on the model described above and the parameters shown in Table 1, we set the input signal of the torque motor as a step signal to observe the effect of different key parameters on the response speed of the 2D electric feedback flow control valve under the no-load condition, as shown in Figure 10.

When the system pressure is 6 MPa, 9 MPa, and 15 MPa, the step response time is 44 ms, 40 ms, and 35 ms, respectively (Figure 11a). Increasing the system pressure will accelerate the response. Because increasing the system pressure reduces the pressure flow gain coefficient, the damping ratio will be reduced, thus increasing its response speed. However, the system pressure reduces the stability of the system.

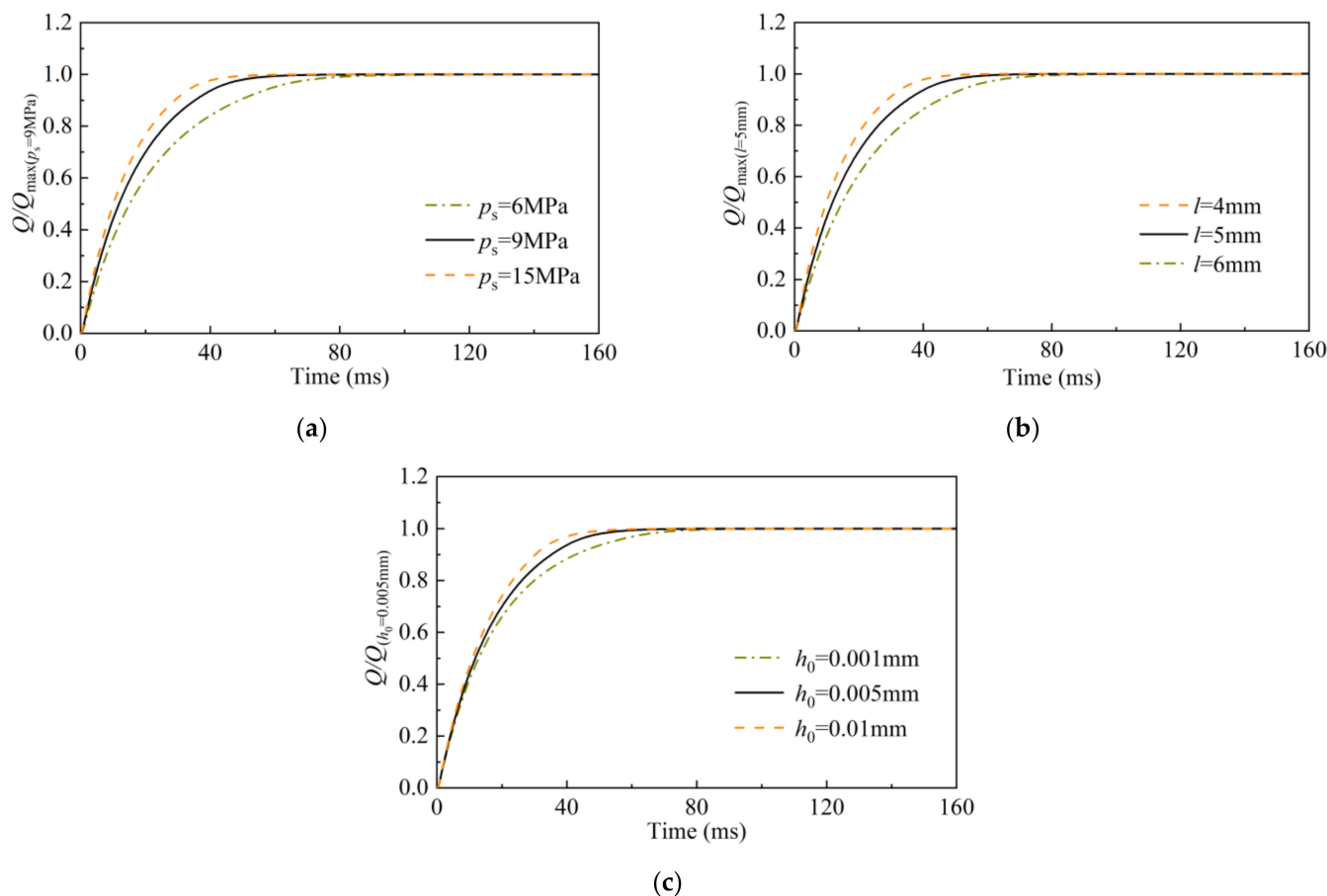


Figure 11. The effect of key parameters on the step response. (a) Effect of system pressure on the step; (b) effect of damping piston length on the step; (c) effect of initial overlap height on the step.

When the damping piston length is 4 mm, 5 mm, and 6 mm, the step response time is 34 ms, 40 ms, and 43 ms, respectively (Figure 11b). As the length of the damping piston increases, the response speed gradually decreases, but it does not affect the steady-state value of the output flow. According to Equation (8), the length of the damping piston is proportional to its damping magnitude. Therefore, increasing the length of the damping piston will increase the damping ratio of the system and result in a slower response. In the meantime, this increase can improve the stability of the system.

If the initial overlap height is 0.001, 0.005, and 0.01 mm, the step response time is 43 ms, 40 ms, and 37 ms, respectively (Figure 11c). As the initial overlap height increases, the flow valve response time decreases, and the response speed increases. According to Equation (6), increasing the initial overlap height will increase the amount of high-pressure oil flowing into the sensitive chamber, and the pressure in the sensitive chamber will change faster, thus increasing the response speed. However, increasing the initial overlap height increases the leakage.

Therefore, adjusting the system pressure, the length of the damping piston, and the initial overlap height of the high- and low-pressure grooves can improve the response speed of the 2D electric feedback flow control valve. Increasing the system pressure and decreasing the length of the damping piston will reduce the stability of the system, whereas increasing the initial overlap height can improve the response speed but will increase the leakage. The step response curve also shows that the 2D electric feedback flow control valve is an over-damped system, and the step curve does not exhibit any oscillation or overshoot.

4.3. Load Characteristic Analysis

To obtain the steady-state characteristic curve of the 2D electric feedback flow regulating the valve spool displacement and output flow rate under flow compensation, we increased the load pressure from 1 MPa to 8 MPa and observed the changes in the main valve spool displacement and outlet flow rate. The simulation results are shown in Figure 12.

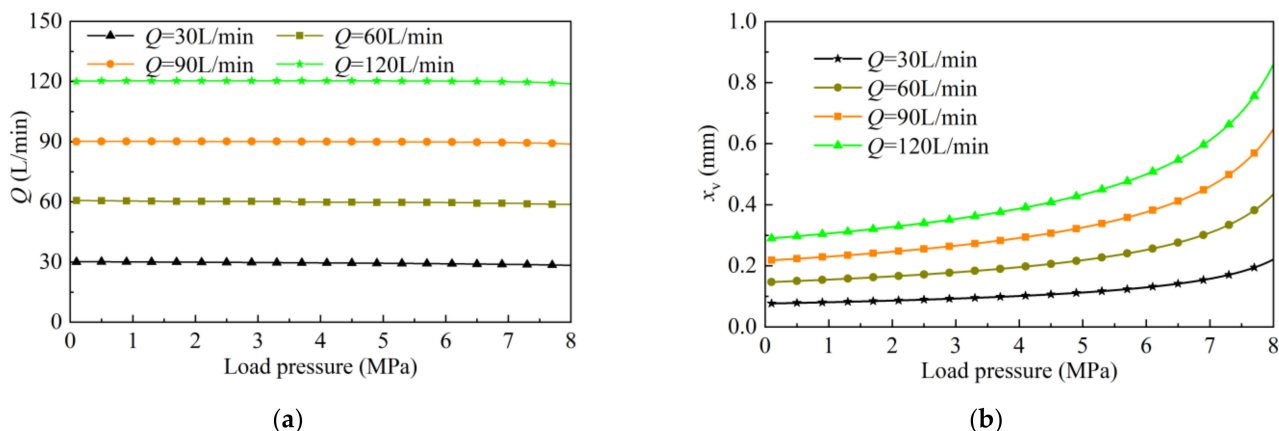


Figure 12. Steady state load characteristic curve. (a) Flow rate variation curve; (b) valve spool displacement variation curve.

The steady-state load flow curve of the 2D electric feedback flow control valve with flow compensation is shown in Figure 12a. The 2D electric feedback flow control valve under flow compensation control has good flow control accuracy, but the flow control accuracy decreases as the load pressure gradually increases. When the input flow signal is 30 L/min, 60 L/min, 90 L/min, and 120 L/min, the maximum errors of the output flow are 2.1%, 1.8%, 1.3%, and 0.8%, respectively. The higher the output-rated flow, the higher the flow control accuracy.

The curve of spool displacement variation of the 2D electric feedback flow control valve under load variation when flow compensation is available is shown in Figure 12b. The spool displacement increases as the load increases. Under the same load variation, the higher the flow rate, the greater the change in the spool displacement.

To understand the load step response characteristics of the 2D electric feedback flow control valve under flow compensation, we conducted a simulation analysis for the same output flow rate and different output flow rates; the simulation results are shown in Figure 13.

Figure 13a shows the dynamic load flow characteristic curve of the 2D electric feedback flow control valve when the inlet pressure of the main valve is kept constant and the load pressure is stepped from 3 MPa to 4 MPa, 5 MPa, and 6 MPa, respectively. When the load pressure rises, the fluctuation of the flow curve also increases, but the adjustment time remains unchanged at approximately 20 ms, and there is no overshoot. After re-entering a steady state, the flow rates before and after the loading step remain.

According to the dynamic load flow characteristic curve of the 2D electric feedback flow control valve (Figure 13b), the output flow rate is 30 L/min, 60 L/min, and 90 L/min, respectively, when the load pressure is increased from 3 MPa to 6 MPa. If the output flow rate was higher, the flow rate fluctuation generated during the load step is also higher. However, the time required for the flow rate to return to the steady state is not affected by the output flow rate, and the output flow rate is unchanged before and after the load step.

Figure 13c shows the effect of the magnitude of damping provided by different differential pressure feedback rod damping pistons on the flow curve for a 2D electric feedback flow control valve output flow rate of 150 L/min and a load pressure step from 3 MPa to 6 MPa. When the damping is larger, the overshoot and oscillation of the flow curve

are smaller, but the response speed decreases. This is because the greater the damping, the slower the differential pressure feedback rod feeds the differential pressure back to the controller. Nonetheless, the displacement of the feedback rod will be more stable. Therefore, the size of the differential pressure rod damping should be optimized to respond to differential pressure changes promptly and ensure a stable flow curve.

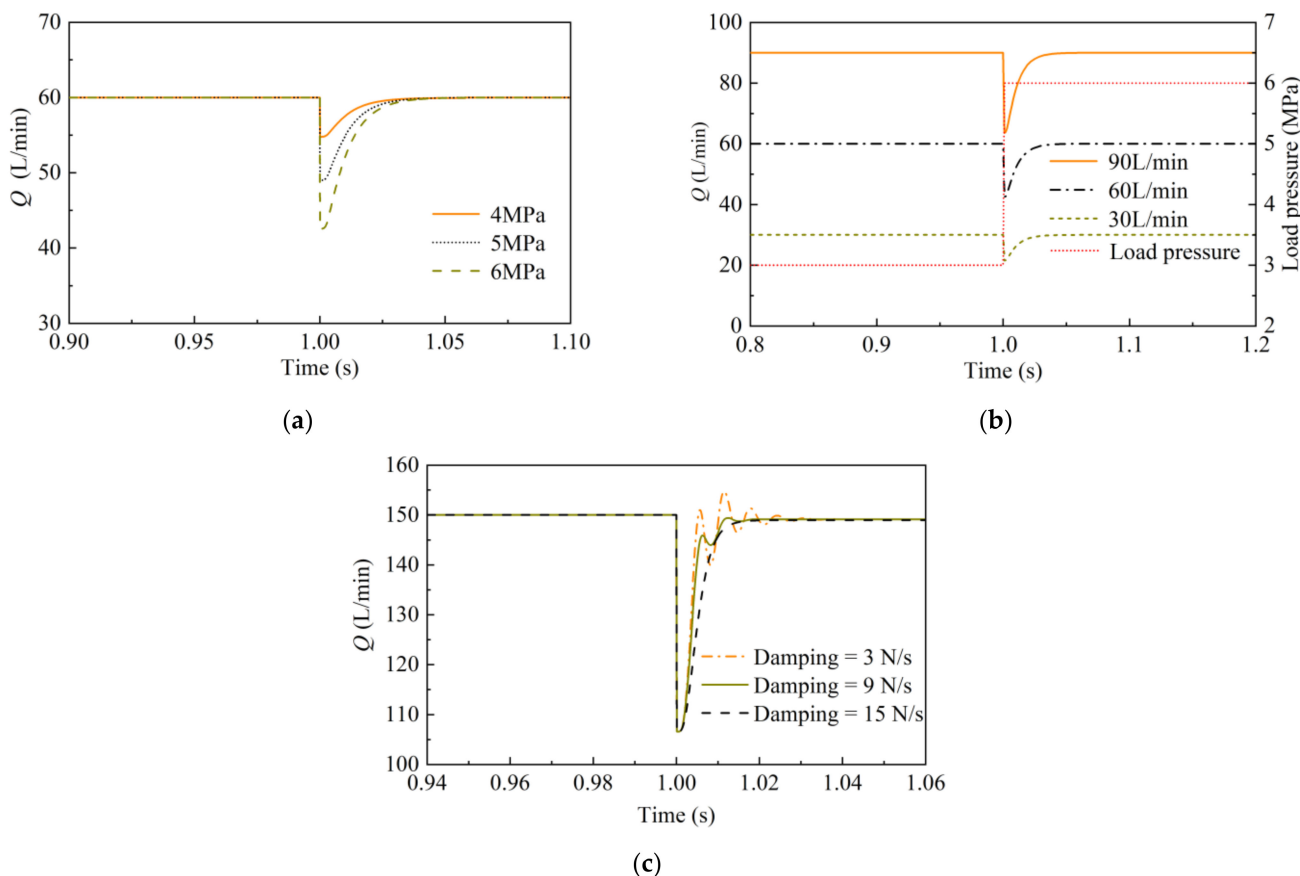


Figure 13. Load step response curve. (a) Effect of different load steps on the flow rate; (b) effect of load steps on different flow rates; (c) load step with different damping.

5. Experimental Studies

5.1. Physical Introduction

The actual size of the 2D electric feedback flow control valve prototype is 70 mm × 70 mm × 147 mm, the mass is 1535 g, and the maximum output flow rate is 200 L/min. The physical object is shown in Figure 14, and the key parameters of the flow valve are shown in Table 3.



Figure 14. Physical diagram of the 2D electric feedback flow control valve.

Table 3. Key parameters of the 2D electric feedback flow control valve.

Parameters	Values
System input oil pressure/MPa	9
Valve spool diameter/mm	25
Valve spool quality/g	96
Inclined trough inclination angle/°	84
2D position diameter/mm	12
High-pressure groove width/mm	5
Initial overlap height/mm	0.005
Damping piston diameter/mm	15.82

5.2. Experimental Platform

We built a relevant experimental platform to experimentally verify the 2D electrical feedback flow control valve. Figure 15 shows a schematic diagram. The equipment of the experimental system mainly includes a signal generator, LVDT linear displacement sensor (model CD375, range 1.26 mm), pressure sensor (model CYYZ11, range 0–40 MPa, accuracy 0.1 MPa), flow meter (model MF1, range 0–200 L/min, accuracy 0.2%), 2D electric feedback flow control valve, oscilloscope, and computer. We used a signal generator to generate the input signal for the experiment. We controlled the torque motor using the controller of a 2D electric feedback flow control valve. The flow meter is used to observe and judge whether the current flow rate meets expectations. The oscilloscope is used to display the operation of each signal. A physical diagram of the experimental platform is shown in Figure 16a; a physical diagram of the experimental equipment is shown in Figure 16b.

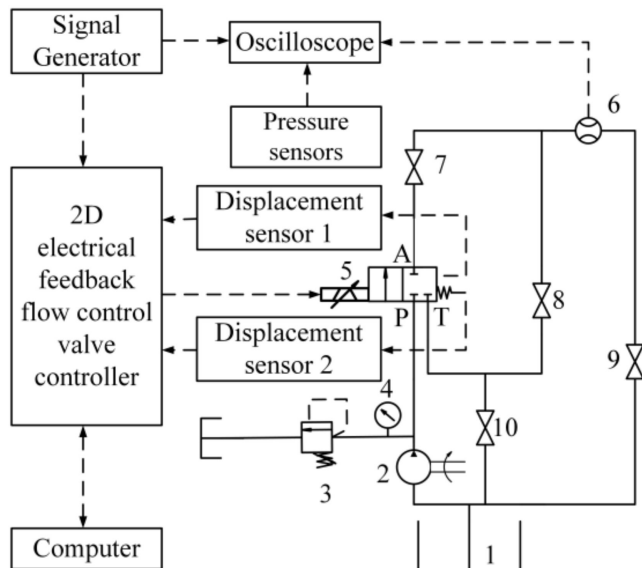


Figure 15. Schematic diagram of the experimental system. 1. oil tank; 2. hydraulic pump; 3. relief valve; 4. pressure gauge; 5. 2D electrical feedback flow control valve; 6. flow meter; 7–10. shut-off valve.

5.3. Static Characteristics

5.3.1. Flow Static Characteristics

To test whether the static characteristics of the 2D electric feedback flow valve meet the design requirements, the system pressure is set to 9 MPa, and the load pressure is 0 MPa. We assigned the signal generator output frequency to a 0.02 Hz sine wave voltage signal, full-scale input, through the flow meter to detect the output flow signal. An oscilloscope was used to record the change in the flow signal with the input signal in multiple cycles, intercepting one of the complete cycles, after collating the experimental data to obtain a 2D electric feedback flow valve flow static characteristic curve (Figure 17).

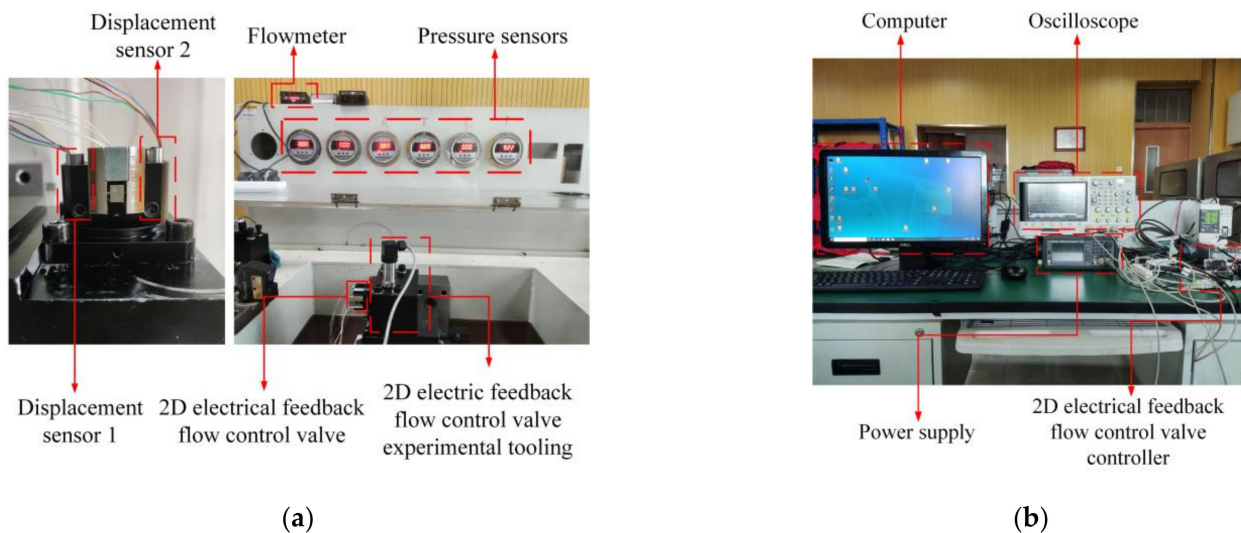


Figure 16. Test bench and some experimental equipment. (a) Actual picture of the experimental platform; (b) real picture of experimental equipment.

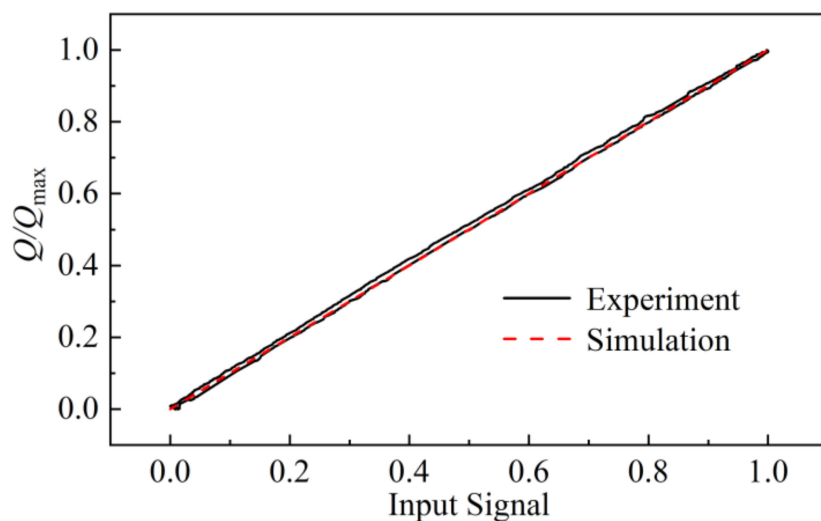


Figure 17. Static flow characteristic curve.

The curves shown in Figure 17 show that the hysteresis size of the 2D electric feedback flow valve is 4.4%, and the linearity is 1.6% under no load. Both meet the design criteria of hysteresis and linearity of less than 5%. The theoretical value is better than the experimental value probably because the hysteresis size of the torque motor is not considered in the simulation, and some parameters are linearized when establishing the displacement angle equation.

5.3.2. Differential Pressure Measurement

In the displacement curve of the differential pressure feedback rod (Figure 18), when the differential pressure changes, the system pressure is 9 MPa. The throttle port size is adjusted so that the 2D electrical feedback flow control valve inlet and outlet pressure drop gradually increased, and this was repeated several times to obtain several groups of differential pressure feedback rod displacements and differential pressures against each other.

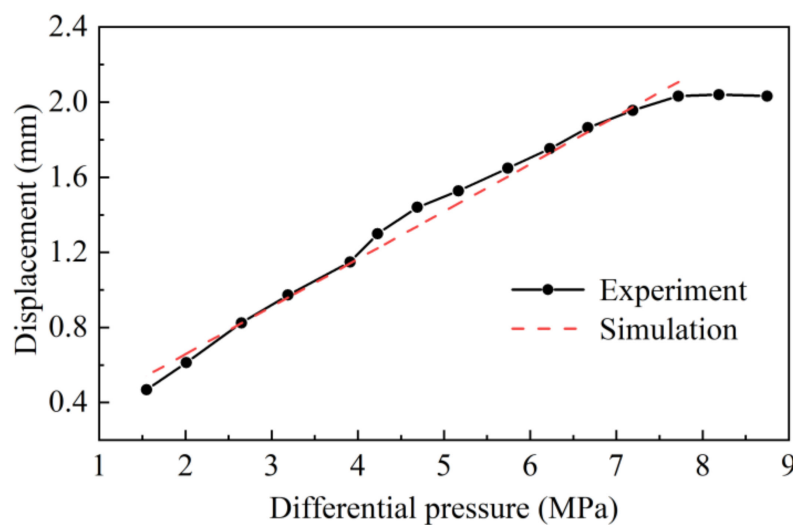


Figure 18. Displacement–differential pressure curve.

In general, the displacement curve of the differential pressure feedback rod is linear, and the individual position is non-linear, which is caused by friction. When the pressure drop of the inlet and outlet increases to approximately 8 MPa, the displacement of the differential pressure feedback rod is almost unchanged because of the limitation of the spring cavity. Therefore, the effective differential pressure measurement range is approximately 8 MPa.

5.4. Dynamic Characteristics

5.4.1. Step Response

Figure 19 shows the step response curve of the 2D electric feedback flow valve, where the system pressure is 9 MPa, the load pressure is 0 MPa, and the signal generator output amplitude is set to a 0–3 V (full-scale input) square wave signal. We recorded the step change in the flow signal, with the input signal recorded using the oscilloscope. The data are normalized.

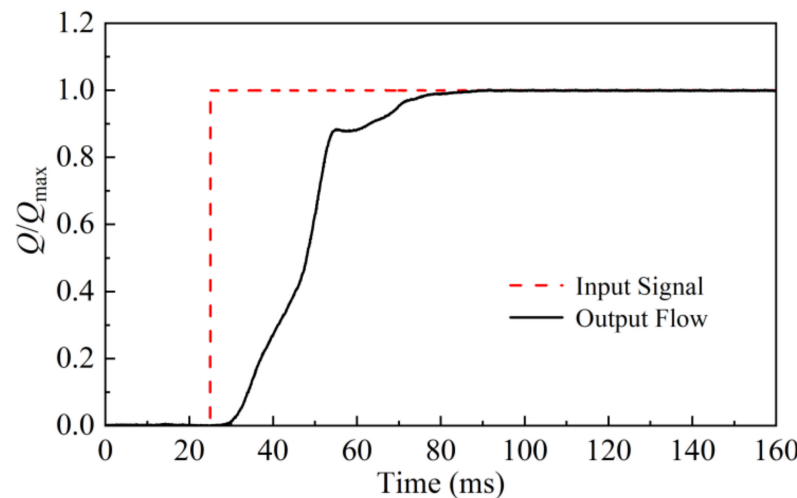


Figure 19. Step response curve.

The step response curve of the 2D electric feedback flow valve is overdamped without any overshoot, which is consistent with the simulation results. The step response time is approximately 44 ms. This meets the design standard of 50 ms but is slower than the simulation result of 40 ms, probably because the simulation does not consider the effect of torque motor hysteresis. The response time of the same level of flow valve is about 50 ms.

The response speed of the 2D electric feedback flow control valve is faster, mainly because of the 2D valve structure and some system optimization such as changing the high- and low-pressure orifices into high- and low-pressure grooves.

5.4.2. Frequency Response

The signal generator is set up to generate a sine wave with an amplitude of 0~0.75 V (25% of full scale), and the frequency of the sine wave is varied. We processed these data to obtain the frequency characteristic curve of amplitude and phase angle with frequency change. When the amplitude ratio decays to 70.7% or the phase lag is 90°, the 2D electric feedback flow control valve no longer has good following characteristics. The following curves at 1 Hz, 5 Hz, 10 Hz, and 20 Hz flow are shown in Figure 20.

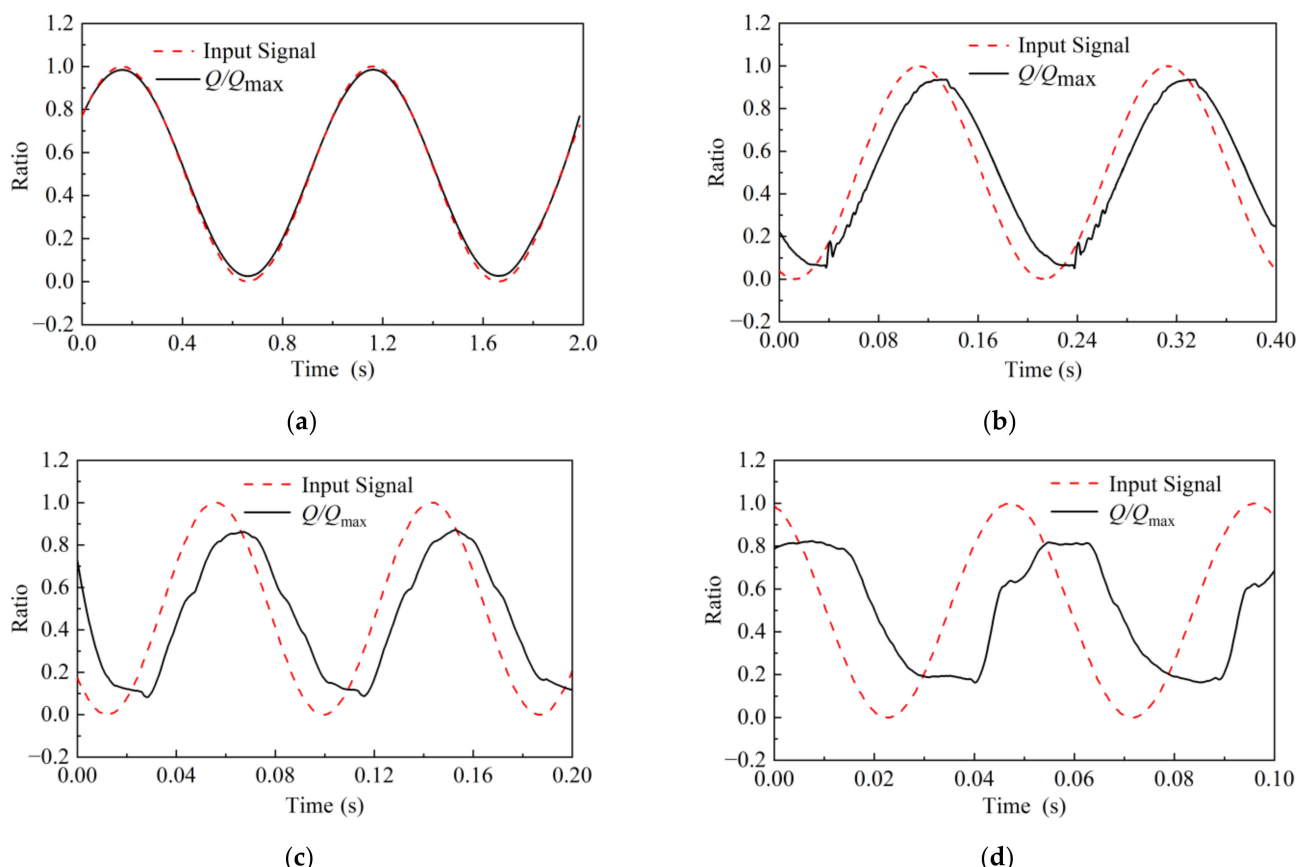


Figure 20. Flow-following curves at different frequencies. (a) Flow-following curve at an input signal frequency of 1 Hz; (b) flow-following curve at an input signal frequency of 5 Hz; (c) flow-following curve at an input signal frequency of 10 Hz; (d) flow-following curve at an input signal frequency of 20 Hz.

Figure 21 shows the frequency characteristic curve of the processed 2D electrical feedback flow control valve. The flow signal of the 2D electro-feedback flow control valve decays to -3 dB at a control signal frequency of about 17 Hz, with a phase lag of 90° at about 28 Hz. Therefore, the actual operating frequency width of the 2D electric feedback flow control valve is 17 Hz, consistent with the simulation results. Compared with the traditional differential-pressure-compensated flow valve, the 2D electrical feedback flow control valve flow valve has a significantly improved and enhanced frequency response.

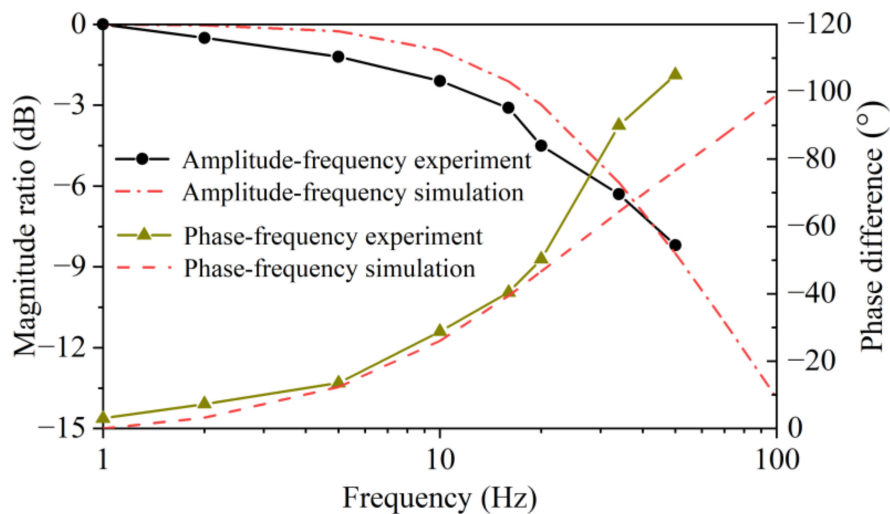


Figure 21. Frequency response curve.

5.5. Flow Stability

To verify the change of flow rate and spool displacement at the valve port when the load pressure at the working port increases, we fixed the input signal and gradually reduced the throttle opening to simulate the load change. We observed the pressure gauge and oscilloscope. When the spool displacement and outlet flow rate return to a steady state, the current values of spool displacement and output flow rate are recorded, and the control relationship between flow rate and spool displacement and load pressure can be obtained by changing the size of the input signal. The experimental results are shown in Figure 22.

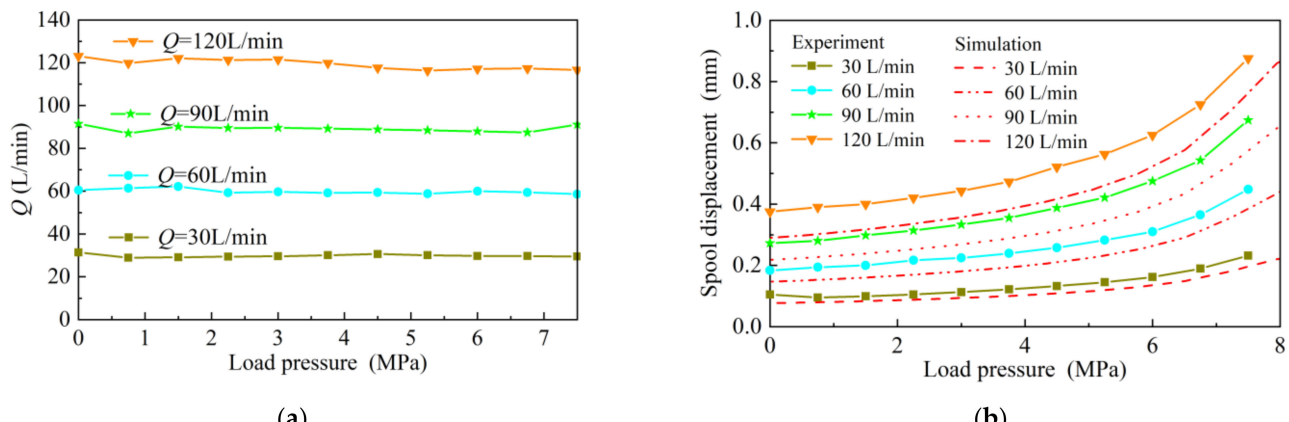


Figure 22. Load characteristic curve. (a) Flow curve under static load variation; (b) spool displacement curve under static load variation.

The 2D electric feedback flow control valve does not change with the increase in load when the load increases from 0 MPa to 7.5 MPa (Figure 22a). When the output flow rate is 30 L/min, 60 L/min, 90 L/min, and 120 L/min, the steady-state errors corresponding to the output flow rate are 7.56%, 6.95%, 4.2%, and 3.43%, respectively. The larger the rated flow rate is, the smaller the steady-state error is. This finding is consistent with the previous simulation results, but the experimental error is larger probably due to some listed factors such as the processing error, pressure feedback accuracy, and oil temperature variation.

The trend of spool displacement is consistent with the previous simulation results, but as the rated flow rate increases, the actual spool displacement is larger compared to the simulation (Figure 22b). This may be caused by machining errors that lead to large differences between the theoretical and actual values of the valve port flow coefficient.

6. Conclusions

In this study, we have proposed a new 2D electrical feedback flow control valve. We further derived, simulated, and verified experimentally the mathematical model using AMESim. Our conclusions are:

- (1) The 2D electric feedback flow control valve not only has a simple structure and a high integration, but also, like the 2D servo valve, it is small, responds fast, and has a strong anti-pollution ability.
- (2) We have analyzed the 2D electrical feedback flow control valve by mathematical model and AMESim simulations. We found that the key parameters of the 2D piston would affect the response speed of the flow valve and verified the feasibility of closed-loop flow through differential pressure feedback rod and spool displacement. Through the simulation, we found that when the rated flow rate is larger, the flow steady-state error is smaller; the stability of the differential pressure feedback lever also affects the flow stability, so one should pay attention to the size of the differential pressure feedback lever damping when designing the prototype.
- (3) We have obtained the suitable key parameters by simulation and processed the prototype for experimental verification. The experimental results show that the 2D electro-feedback flow control valve has good dynamic, static characteristics, and flow stability. Compared with the same type of electric feedback flow valve, such as the flow control valve proposed previously [13], the 2D electric feedback flow control valve we proposed has better dynamic characteristics and a smaller size.

Author Contributions: Prototype design modeling, J.Z.; guidance, S.L. and W.J.; simulation, Q.D.; experiments, Q.D. and J.Z.; resources, S.L.; data organization, Q.D.; writing—original draft preparation, Q.D.; writing—review and editing, Q.D.; supervision, W.J.; project management, S.L.; funding acquisition, S.L. All authors have read and agreed to the published version of the manuscript.

Funding: This research was funded by The National Key Research and Development Program of China, grant number 2019YFB2005201.

Data Availability Statement: Not applicable.

Conflicts of Interest: The authors declare no conflict of interest. The funders had no role in the design of the study; in the collection, analyses, or interpretation of data; in the writing of the manuscript, or in the decision to publish the results.

Appendix A

The parameters used in the equations in this paper have been listed in the following table.

Table A1. Table of parameters collection.

Parameters	Paraphrase
A_o	Effective force area on the right side of the pressure-sensing piston
A_i	Effective force area on the left side of the pressure-sensing piston
K_q	Pressure measuring spring stiffness
Δx	Magnitude of the differential pressure feedback rod displacement
A_1	Overlap area between the high-pressure groove and the oblique groove
A_2	Overlap area between the low-pressure groove and the oblique groove
p_k	Oil outlet pressure
p_s	Oil inlet pressure
K_q	Pressure measuring spring stiffness
Δx	Differential pressure feedback rod displacement
R	2D piston radii

Table A1. *Cont.*

Parameters	Paraphrase
β	Inclination angle of the oblique groove
θ	2D piston rotation angle
h_0	Initial overlap height of the high-pressure trough and the inclined trough
x_v	Spool displacement
q_1	Flow rate from the high-pressure groove to the sensitive chamber via the oblique groove
q_2	Flow rate of the sensitive chamber into the low-pressure groove
A_s	Effective area of the sensitive chamber pressure on the 2D piston
V_c	Volume of sensitive chamber
β_e	Bulk modulus of elasticity of the oil
p_c	Sensitive chamber pressure
C_d	Flow coefficient
w	Width of the high- and low-pressure grooves
ρ	Fluid density
μ	Viscosity coefficient of the oil
l	Thickness of the damping piston
D	Large diameter of the damping piston
d	Small diameter of the damping piston
y_0	Oil film thickness
ω_n	Intrinsic frequency of the 2D valve piston
K_1	2D valve piston flow gain coefficient
K_2	2D valve piston pressure flow gain coefficient
ζ_n	2D valve piston damping ratio
Q	Valve port flow
ω	Gradient of the valve port through-flow area
Δp	Differential inlet and outlet pressure

References

- Cheng, M. Modeling and analysis of a pressure compensated flow control valve. In Proceedings of the ASME Fluids Engineer Summer Meeting, Houston, TX, USA, 19–23 June 2005.
- Murrenhoff, H. Trends in Valve Development. In *O+P Ölhydraulik und Pneumatik*; Vereinigte Fachverlage: Mainz, Germany, 2003; Volume 46, pp. 1–36.
- Mao, Z.; Yoshida, K.; Kim, J. A micro vertically-allocated SU-8 check valve and its characteristics. *Microsyst. Technol.* **2018**, *25*, 245–255. [[CrossRef](#)]
- Lin, T.; Lin, Y.; Ren, H. A double variablecontrol load sensing system for electric hydraulic excavator. *Energy* **2021**, *233*, 119999. [[CrossRef](#)]
- Wu, D.; Burton, R.; Schoenau, G.; Bitner, D. Analysis of a pressurecompensated flow control valve. *J. Dyn. Syst. Meas. Control.* **2007**, *129*, 203–211. [[CrossRef](#)]
- Lu, Y. New progress in flow control technology. *Chin. Hydraul. Pneum.* **1982**, *2*, 23–29.
- Kuehnlein, M.; Liermann, M.; Ewald, J.; Murrenhoff, H. Adjustable Flow-Control Valve for the Self-Energising Electro-Hydraulic Brake. *Int. J. Fluid Power* **2012**, *13*, 5–14. [[CrossRef](#)]
- Okhotnikov, I.; Noroozi, S.; Sewell, P.; Godfrey, P. Evaluation of steady flow torques and pressure losses in a rotary flowcontrol valve by means of computational fluid dynamics. *Int. J. Heat Fluid Flow* **2017**, *64*, 89–102. [[CrossRef](#)]
- Wang, J.; Liu, X.; Wang, Z.; Chen, J.; Han, Y.; Wang, Y. Flow characteristics analysis of constant flow control valve based on AMESim. *J. Jilin Univ. (Eng. Technol. Ed.)* **2022**, *1*–9. [[CrossRef](#)]
- Jin, B.; Zhu, Y.; Li, B.; Zhang, D.; Zhang, L.; Chen, F. A differential control method for the proportional directional valve. *J Zhejiang Univ. Sci. C (Comput. Electron.)* **2014**, *1*, 892–902. [[CrossRef](#)]
- Milecki, A.; Ortmann, J. Electrohydraulic linear actuator with two stepping motors controlled by overshoot-free algorithm. *Mech. Syst. Signal Process.* **2017**, *96*, 45–57. [[CrossRef](#)]
- Wang, B.; Liu, H.; Hao, Y.; Quan, L.; Li, Y.; Zhao, B. Design and Analysis of a Flow-Control Valve with Controllable Pressure Compensation Capability for Mobile Machinery. *IEEE Access* **2021**, *9*, 98361–983682021. [[CrossRef](#)]
- Li, M.; Ye, J.; Xie, B.; Yang, S.; Zeng, B.; Liu, J. Design and Test of Hydraulic Proportional Flow Valve forHydraulic Chassis in Tractor. *Trans. Chin. Soc. Agric. Mach.* **2018**, *49*, 397–403. [[CrossRef](#)]
- Huang, J.; Dai, J.; Quan, L.; Lan, Y. Performance of proportional flow valve with pilot pressure drop–spool opening compensation. *J. Dyn. Syst. Meas. Control.* **2017**, *139*, 011009. [[CrossRef](#)]
- Zhao, B.; Quan, L.; Huang, J.; Zhang, Y. Characteristics of Electro-hydraulic Proportional Valve with Pilot Pressure Variation-Displacement Adjustment. *Chin. J. Mech. Eng.* **2017**, *53*, 195–201. [[CrossRef](#)]

16. Hao, Y.; Quan, L.; Huang, J. Research on the performance of electro-hydraulic proportional flow valve controlled by active pilot pump. *Proc. Inst. Mech. Eng. Part E* **2017**, *231*, 720–731. [[CrossRef](#)]
17. Huang, J.; Wang, X.; Wang, H.; Hao, H. Development of a flow control valve with digital flow compensator. *Flow Meas. Instrum.* **2019**, *66*, 157–169. [[CrossRef](#)]
18. Zhang, J.; Deng, Y.; Zhang, N.; Zhang, B.; Qi, H.; Zheng, M. Vibration Performance Analysis of a Mining Vehicle with Bounce and Pitch Tuned Hydraulically Interconnected Suspension. *Chin. J. Mech. Eng.* **2019**, *32*, 195–211. [[CrossRef](#)]
19. Xu, Y.; Liu, X.; Xu, J. Research on the Structural Rigidity Characteristics of a Reconfigurable TBM Thrust Mechanism. *Chin. J. Mech. Eng.* **2019**, *32*, 45–57. [[CrossRef](#)]
20. Ruan, J.; Burton, R.; Ukrainetz, P. An Investigation into the Characteristics of a Two Dimensional “2D” Flow Control Valve. *J. Dyn. Syst. Meas. Control.* **2002**, *124*, 214–220. [[CrossRef](#)]
21. Ruan, J.; Ukrainetz, P.; Burton, R. Frequency domain modeling and identification of 2D digital servo valve. *Int. J. Fluid Power* **2000**, *1*, 76–85. [[CrossRef](#)]
22. Long, Q.; Ruan, J.; Li, S.; He, J. Stability of 2D pressure servo valve considering cavitation effect. *Acta Aeronaut. Astronaut. Sin.* **2020**, *41*, 423281. Available online: <https://kns.cnki.net/kcms/detail/11.1929.V.20190917.1003.012.html> (accessed on 17 September 2019).

Disclaimer/Publisher’s Note: The statements, opinions and data contained in all publications are solely those of the individual author(s) and contributor(s) and not of MDPI and/or the editor(s). MDPI and/or the editor(s) disclaim responsibility for any injury to people or property resulting from any ideas, methods, instructions or products referred to in the content.